

# Chiral-odd transversity spin structure function $h_1(x)$ of the nucleon in a constituent quark model

Katsuhiko Suzuki\*

*Institut für Theoretische Physik, Technische Universität München*

*D-85747 Garching, Germany*

and

Takayuki Shigetani†

*Computation Center, The Institute of Physical and Chemical Research (RIKEN)*

*Wako, Saitama 351-01, Japan*

## Abstract

We study the chiral-odd transversity spin-dependent quark distribution function  $h_1(x)$  of the nucleon in a constituent quark model. The twist-2 structure functions,  $f_1(x)$ ,  $g_1(x)$  and  $h_1(x)$  are calculated within the diquark spectator approximation. Whereas an inequality  $f_1(x) > h_1(x) > g_1(x)$  holds with the interaction between quark and diquark being scalar, the axial-vector effective quark-diquark interaction, which contributes to the  $d$ -quark distribution, does not lead to such a simple relation. We find that  $h_1(x)$  for the  $d$ -quark becomes somewhat smaller than  $g_1^d(x)$ , when we fix the model parameter to reproduce known other structure functions. We also include corrections due to the non-trivial structure of the constituent quark, which is modeled by the Goldstone boson dressing. This improves agreements of  $f_1(x)$  and  $g_1(x)$  with experiments, and brings further reduction of  $h_1^d(x)$  distribution. Consequences for semi-inclusive experiments are also discussed.

Key Words: structure function, nucleon spin, constituent quark model, chiral symmetry

---

\*Alexander von Humboldt fellow, e-mail address : ksuzuki@physik.tu-muenchen.de

†e-mail address : shige@postman.riken.go.jp

## 1 Introduction

Study of the nucleon spin structure triggered by the unexpected EMC result [1] becomes one of the most challenging issues in the hadron physics. The spin structure function obtained by the polarized lepton-hadron deep inelastic scattering tells us a lack of our understandings of the quark and gluon dynamics in the nucleon. From the lepton-hadron deep inelastic scattering, one can obtain the longitudinal spin structure function  $g_1(x)$ [2] and the transverse spin structure function,  $g_2(x)$ , which contains information on twist-3 pieces[3]. These structure functions reveal the helicity distribution function as well as the quark-gluon correlation in the nucleon[4]. Further approach using the semi-inclusive process is now planned, which makes it possible to know detailed decomposition of the nucleon spin structure.

Recently, chiral-odd structure function is discussed as complementary tool to study the structure of the nucleon[5, 6]. In the lepton-hadron scattering, in which the chirality is conserved, only the chiral-even structure functions can be observed. On the other hand, in the Drell-Yan process, the chirality changing process is possible, and thus the chiral-odd structure function is expected to be measured.

In terms of the quark-quark density matrix, the twist-2 structure functions of the nucleon are expressed as[6],

$$\int \frac{d\lambda}{2\pi} e^{i\lambda x} \langle P, S | \psi(0) \gamma_\mu \psi(\lambda n) | P, S \rangle = 2 [f_1(x) + \text{h.t.}] \quad (1)$$

$$\int \frac{d\lambda}{2\pi} e^{i\lambda x} \langle P, S | \psi(0) \gamma_\mu \gamma^5 \psi(\lambda n) | P, S \rangle = 2 [g_1(x) P_\mu (S \cdot n) + \text{h.t.}] \quad (2)$$

$$\int \frac{d\lambda}{2\pi} e^{i\lambda x} \langle P, S | \psi(0) \sigma_{\mu\nu} i\gamma^5 \psi(\lambda n) | P, S \rangle = 2 [h_1(x) (S_{\perp\mu} P_\nu - S_{\perp\nu} P_\mu) + \text{h.t.}] \quad (3)$$

(h.t. denotes the higher twist contributions.)

Here, we followed the definition of Ref. [6].  $f_1(x)$  is the usual spin-independent quark distribution, and  $g_1(x)$  the quark helicity distribution function in the longitudinally polarized nucleon. These two distribution functions are chiral-even, and can be measured by the lepton-hadron scattering. The *transversity* spin distribution function  $h_1(x)$  is chiral-odd, in which we are mainly interested in this paper. The  $h_1(x)$  structure function corresponds to a target helicity-flip amplitude in the helicity basis, and thus does not have simple partonic probabilistic interpretation. As pointed out in Ref. [6], however, the transversity spin distribution can be understood as difference

of numbers of valence quarks with eigenvalues  $+1$  and  $-1$  of the transverse Pauli-Lubanski operator in the transversely polarized nucleon.

Our aim of this paper is to present  $h_1(x)$  using low energy effective quark model, which is already used to calculate known structure functions  $f_1(x)$  and  $g_1(x)$ . In particular, we discuss the flavor dependence of the transversity spin distribution  $h_1(x)$  in detail, compared with other twist-2 quark distributions. We evaluate quark distribution functions  $f_1(x)$ ,  $g_1(x)$  and  $h_1(x)$  of the nucleon based on a constituent quark picture, which is successful to describe the low energy hadron properties. Here, current quarks are assumed to acquire their dynamical masses due to spontaneous breakdown of the chiral symmetry following to the Nambu and Jona-Lasinio model[7]. We take the model developed in Ref. [8, 9, 10] to calculate the structure functions, where the nucleon is described as a bound state of the quark and diquark.

For effective interaction between quark and diquark, we take both scalar and axial-vector types from the symmetry consideration. In principle, we could solve a bound state equation of the quark-diquark for the nucleon. However, it needs difficult procedure, and is first recently done by Kusaka *et al.* for only the scalar channel[11]. Here, we simply assume reasonable forms of the quark-diquark vertex functions for the scalar and axial-vector channels so as to reproduce the observed structure function  $f_1(x)$  and  $g_1(x)$ , and try to describe  $h_1(x)$  structure function.

There are several works to investigate the transversity spin distribution function  $h_1(x)$  within the quark models[6, 12, 13, 14]. Since  $h_1(x)$  is defined by the chirality-violating operator, the transversity spin structure function may depend on the chiral-odd operators of the theory, *e.g.* the quark condensate of the QCD vacuum[12].

Recently, Soffer has proposed that such twist-2 quark distribution functions,  $f_1(x)$ ,  $g_1(x)$  and  $h_1(x)$ , are subject to *Soffer's inequality*, which is derived from a general argument[15, 16].

$$f_1(x) + g_1(x) \geq 2|h_1(x)| \quad (4)$$

We discuss behavior of this inequality in our model.

In particular, the simple relativistic quark model such as the bag model[6], where the relativistic quarks independently move inside the confinement region, leads to a relation;

$$f_1(x) + g_1(x) = 2|h_1(x)| \quad (5)$$

$$|h_1(x)| > |g_1(x)| \quad (6)$$

The first equation (5) means a saturation of the Soffer's inequality in the model, discussed by Goldstein *et al.*[16]. The second inequality comes from roles of the lower component of the Dirac spinor. Indeed, 1st moments of  $g_1(x)$  and  $h_1(x)$ , axial charge and tensor charge, are given by

$$\begin{aligned} \Delta q &= \int [dr] \left[ F^2 - \frac{1}{3} G^2 \right] \\ \delta q &= \int [dr] \left[ F^2 + \frac{1}{3} G^2 \right] \end{aligned}$$

where  $F$  and  $G$  are upper and lower radial wave functions of the Dirac spinor. Eq. (6) is a universal relation of the relativistic quark potential model independent of the model parameters.

However, recent lattice QCD simulation indicates the 1-st moment of the  $|h_1(x)|$  is larger than that of  $|g_1(x)|$  for the  $d$ -quark distribution function[17]. In addition, the QCD sum rule study suggests a very small value of the  $d$ -quark tensor charge[14].

In the present study, we take both scalar and axial-vector quark-diquark-nucleon vertices, and examine such relations. When the nucleon is a bound state of the quark and the scalar diquark, we exactly obtain  $f_1(x) + g_1(x) = 2h_1(x)$  and  $h_1(x) > g_1(x)$ [18], which is quite similar with the bag model calculations. However, for the axial-vector vertex case, which determines the  $d$ -quark distribution function, such simple relations are not maintained. We find  $|h_1^d(x)| < |g_1^d(x)|$  or they are comparable at least, if we fix the model parameters to reproduce the other structure functions.

We also study corrections to the quark distributions from dressed structure of the constituent quark. Constituent quarks are assumed to be quasi-particles of the QCD vacuum, and have non-trivial structure. We introduce the Goldstone boson cloud,  $\pi, K, \eta$ , around the constituent quark studied in Ref. [19]. Such a dressing produces crucial effects on the structure function, namely, reduces a probability to find a bare quark state and also changes the spin structure by emitting the GS boson to relative  $P$ -wave state. Combining these contributions with the results of quark-diquark model, we show that shape of the transversity spin distributions are considerably different from those of the helicity distributions.

This paper is organized as follows. In Section 2, we calculate the chiral-odd type forward scattering amplitude introduced in Ref. [12], which provides the transversity

spin distribution  $h_1(x)$ . Relations of three structure function are examined in some detail. In Section 3, numerical results are given performing the  $Q^2$  evolution of the distribution functions.  $f_1(x)$  and  $g_1(x)$  are compared with the experimental data, and  $h_1(x)$  is presented for forthcoming experiment. We introduce the dressed structure of the constituent structure due to the Goldstone boson cloud, developed recently by Suzuki and Weise[19]. Inclusion of the GS boson dressing improves the agreements substantially. Final section is devoted to summary and discussions.

## 2 Calculations of the twist-2 quark distribution functions

Purpose of the present paper is to study the structure function measured at high energies by means of the low energy quark model of the nucleon. Basic procedure to connect calculations of the quark model with the high energy experimental data is summarized as follows [20]; We evaluate twist-2 matrix elements of the structure function within the effective quark model at the scale  $\mu \sim 1\text{GeV}$ , where the effective models are supposed to work. Calculated structure function has no physical meaning at this scale  $\mu$ , but plays a role of the boundary condition for the QCD evolution equation. With the help of the perturbative QCD, the results are evolved from the low energy model scale  $\mu$  to the high momentum scale, at which the experimental data exist. Higher twist contributions can be neglected, since we are interested in the Bjorken limit  $Q^2 \rightarrow \infty$ . Comparison of the model calculations with the experimental data reveals non-perturbative dynamics in the deep inelastic experiments.

Let us start calculating nucleon structure functions,  $f_1(x)$ ,  $g_1(x)$  and  $h_1(x)$ . We adopt the phenomenological quark-diquark model for the nucleon [8, 9, 10]. In this approach, the virtual photon-nucleon forward scattering amplitude is illustrated in Fig.1. Here, the constituent quark is struck out by the high momentum virtual photon with a residual diquark being spectator. We treat diquarks as only the spectators, though the structure of the diquark itself might be crucial when we go beyond the diquark spectator approximation [9]. Regarding the nucleon-quark-diquark effective vertex, we deal with both scalar and axial-vector types, which are suggested by the success of the  $SU(6)$  spin-flavor symmetry approach.

$$V_S = \mathbf{1}\phi_S(p^2) \tag{7}$$

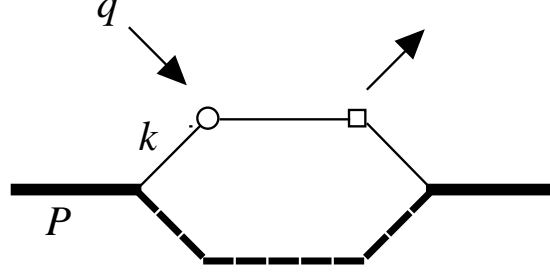


Figure 1: The forward scattering amplitude in the quark-diquark model

The thick and thin solid lines denote the nucleon and the quark, respectively. The spectator diquark is depicted by the dashed line. The circle and box indicate the external currents, which are the axial-vector and scalar currents for  $h_1(x)$ . For  $f_1(x)$  and  $g_1(x)$  cases the current probes the nucleon structure as the vector and axial-vector, respectively.

$$V_V^\mu = \gamma^\mu \gamma^5 \phi_V(p^2) \quad (8)$$

where  $\phi_S(p^2)$  and  $\phi_V(p^2)$  are momentum cutoff functions, specified later.

In the following studies, we use standard definitions for the quark distribution functions[6],

$$F_1(x) = \frac{1}{2} e_a^2 [f_1^a(x) + f_1^{\bar{a}}(x)]$$

where  $F_1(x)$  is the standard electro-production structure function, and  $e_a$  is the electric charge of the quark. Summation  $a$  is over quarks for all flavors.

At first, we show basic steps to derive the spin independent distribution  $f_1(x)$  for the scalar channel. Explicit expressions for  $f_1(x)$  and  $g_1(x)$  are already given in literature[8, 10]. We define the virtual photon-nucleon forward scattering amplitude as,

$$T_{\mu\nu}(q, P, s) = i \int \frac{d^4\xi}{(2\pi)^4} e^{iq \cdot \xi} \langle P, s | T J_\mu(\xi) J_\nu(0) | P, s \rangle \quad (9)$$

where  $J_\mu$  is the vector current. Here,  $q$  is the momentum of the virtual photon, and  $p$  the nucleon momentum with the mass  $P^2 = M^2$ .  $s$  is the nucleon spin, which satisfies  $p \cdot s = 0$  and  $s^2 = -1$ . We also introduce variables,  $\nu = P \cdot q/M$  and the Bjorken- $x$   $x = -q^2/2M\nu = Q^2/2M\nu$ . By virtue of the optical theorem, this forward scattering amplitude is related with the hadronic tensor, which provides the structure function.

In this model, the matrix element is calculated as,

$$T_{\mu\nu} = i \int \frac{d^4 p}{(2\pi)^4} \frac{1}{2} \text{Tr} \left[ V_i(k) S(k) \gamma_\mu S(k+q) \gamma_\nu S(k) V_i(k) D_i(k_2) (\not{P} + M) (1 + \gamma^5 \not{\epsilon}) \right] \quad (10)$$

where momenta delivered by the quark and diquark are  $k$  and  $k_2 = P - k$ , respectively.

Here, the quark propagator  $S(p)$  with the constituent quark mass  $m$  is written as,

$$S(p) = \frac{1}{\not{p} - m} \quad (11)$$

The scalar (spin-0) diquark propagator is given by,

$$D_S(p) = \frac{1}{p^2 - m_D^2}, \quad (12)$$

and for the axial-vector (spin-1) diquark

$$D_V(p)_{\mu\nu} = \frac{1}{p^2 - m_D^2} \left( -g_{\mu\nu} + \frac{p_\mu p_\nu}{p^2} \right) \quad (13)$$

Here,  $m_D$  is masses of the diquarks.

Using the identity,

$$\gamma_\mu \not{q} \gamma_\nu = S_{\mu\rho\nu\sigma} q^\rho \gamma^\sigma - i \varepsilon_{\mu\nu\rho\sigma} q^\rho \gamma^\sigma \gamma^5,$$

one can get the spin independent and dependent distribution functions after suitable projection[4]. For instance, using the projector  $\mathcal{P}_{\alpha\beta} = \frac{1}{4} \left[ \frac{2x}{P \cdot q} P_\alpha P_\beta - g_{\alpha\beta} \right]$ , we can get the unpolarized quark distribution  $f_1(x)$ .

We introduce the light-cone variable,  $x^\pm \equiv x^0 \pm x^3$ . Non-vanishing contribution to the imaginary part of the forward scattering amplitude arises from poles of the struck quark propagator  $[(k+q)^2 - m^2]$  and the spectator diquark propagator  $[k_2^2 - m_D^2]$ . The former is reduced to a condition that the Bjorken- $x$  is identified with the longitudinal momentum fraction of the parton.

$$\delta[(k+q)^2 - m^2] = \frac{1}{2P \cdot q} \delta \left[ \frac{k^+}{P^+} - x \right]$$

The latter one yields,

$$\delta[k_2^2 - m_D^2] = \delta[(1-x)P^+ k_2^- - k_T^2 - m_D^2].$$

Inserting the above results into Eq. (10), one finds

$$\begin{aligned} f_S(x) &= \int \frac{dk^+ dk^- d^2 k_T}{2(2\pi)^4} \frac{\phi_S^2}{(k^2 - m^2)^2} 2\pi \delta \left[ k_2^- - \frac{k_T^2 + m_D^2}{(1-x)P^+} \right] \\ &\quad \times \frac{2\pi \delta(k^+ - xP^+)}{2P \cdot q} \frac{1}{2} \text{Tr}[(\not{k} + m) \not{q} (\not{k} + m) (\not{P} + M)] \\ &= \int_{-\infty}^{k_{\text{max}}^2} \frac{dk^2}{8\pi^2} \frac{\phi_S^2(k^2)}{(k^2 - m^2)^2} \\ &\quad \times [x(M^2 + 2mM - m_D^2) + m^2 - (1-x)k^2] \end{aligned} \quad (14)$$

where

$$k_{\max}^2 = -\frac{x}{1-x}m_D^2 + xM^2 \quad . \quad (15)$$

It is possible to rewrite Eq. (14) as

$$f_S(x) = \int_{-\infty}^{k_{\max}^2} \frac{dk^2}{8\pi^2} \frac{\phi_S^2(k^2)}{(k^2 - m^2)^2} [(xM + m) + k_T^2] \quad (16)$$

with the transverse momentum  $k_T$  given by

$$k_T^2 = (1-x)xM^2 - xm_D^2 - (1-x)k^2$$

Now we come back to the chiral-odd distribution function  $h_1(x)$ , which can not be probed by the electro-magnetic current, as mentioned in Section 1. Ioffe and Khodjamirian introduced the following scattering amplitude[12], which allows us to evaluate  $h_1(x)$  as,

$$T_\mu(q, P, s) = i \int d^4\xi e^{iq \cdot \xi} \frac{1}{2} \langle P, s | T \{ J_{\mu 5}(\xi) J(0) + J(\xi) J_{\mu 5}(0) \} | P, s \rangle \quad (17)$$

where we choose the transverse nucleon spin  $s = (0, 1, 0, 0)$ . This forward scattering amplitude is related with the  $h_1(x)$  structure function.

$$\begin{aligned} T_\mu(q, P, s) = & \left( s_\mu - \frac{P \cdot q}{q^2} q_\mu \right) \tilde{h}_1(x) \\ & + \left( P_\mu - \frac{P \cdot q}{q^2} q_\mu \right) (q \cdot s) \tilde{l}_1(x) + \varepsilon_{\mu\nu\lambda\sigma} q_\lambda s_\sigma (q \cdot s) \tilde{l}_2(x) \end{aligned} \quad (18)$$

Hence, one can obtain the transversity spin distribution function through the optical theorem;

$$h_1(x) = -\frac{1}{\pi} \text{Im} \tilde{h}_1(x) \quad (19)$$

Straightforward calculations yield the following expression for the scalar spin-0 di-quark spectator process[18];

$$h_S(x) = \int_{-\infty}^{k_{\max}^2} \frac{dk^2}{8\pi^2} \frac{\phi_S(k^2)}{(k^2 - m^2)^2} [(xM + m)^2] \quad (20)$$

where we use  $(k \cdot s)^2 = k_x^2 = k_T^2/2$ . It is interesting to note that resulting  $h_S(x)$  is proportional to masses of the nucleon  $M$  and the constituent quark  $m$ , which are the chiral symmetry breaking parameter of the model. If we assume a ‘un-realistic’ chiral symmetric world,  $M = m = 0$ , the  $h_S(x)$  distribution function vanishes. This



is different from  $f_1(x)$  and  $g_1(x)$ , which are non-zero even if all the particles are mass-less.

Using (11) and (13) and summing spin-1 diquark helicities, we also get the  $h_1(x)$  for the axial-vector diquark spectator process.

$$h_V(x) = \int_{-\infty}^{k_{\max}^2} \frac{dk^2}{(8\pi^2)} \frac{\phi_V(k^2)}{(k^2 - m^2)^2} \left[ -x(M - m)^2 + \frac{1}{m_D^2} \left[ (k^2 - m^2)(k^2 - M^2) + x(k^2 - M^2)(m^2 - M^2) - k_T^2(m + M)^2 \right] \right] \quad (21)$$

It is not easy to see how  $h_1^d(x)$  behaves in the chiral mass-less limit. Even if we take  $m = M = 0$ , a term  $\sim k^4/m_D^2$  survives and  $h_V(x) \neq 0$ .

Before constructing the nucleon structure function with the explicit spin-flavor wave function, we shall discuss relations of these quark distribution functions and the Soffer's inequality[15]. We show in Fig.2  $f_S(x)$ ,  $g_S(x)$  and  $h_S(x)$  calculated by the quark-scalar diquark model. In this case, the relation  $f_S(x) > h_S(x) > g_S(x)$  holds, independent of the model parameters, and the Soffer's inequality is saturated  $f_S(x) + g_S(x) = 2h_S(x)$ . This behavior is similar with the bag model.

The spin-1 diquark spectator process shows rather non-trivial behavior. The quark distribution functions are shown in the middle of Fig.2. The Soffer's inequality is satisfied, but can not be saturated. Moreover, relative magnitude of  $g_V(x)$  and  $h_V(x)$  depends on the choice of the parameters. Here, we use the parameter set, which is suitable to reproduce other quantities such as the quark momentum fraction and  $g_A$ . We can not find any simple relation for  $h_V(x)$  and  $g_V(x)$ . For completeness, we plot  $f(x) + g(x) - 2|h(x)|$  in a lower part of Fig.2. In the spin-0 diquark spectator case, this quantity becomes exactly zero, which means a saturation of Soffer's inequality. Result of the spin-1 diquark case also satisfies a positive condition for  $f(x) + g(x) - 2|h(x)|$ .

In terms of these distribution functions, we construct the nucleon structure functions with the spin and flavor structure. Since we have already included the spin structure of the diquarks to calculate the distribution functions and summed up over diquark helicities, we need only flavor structure of the nucleon wave function, which is given by

$$|p\rangle = \frac{1}{\sqrt{2}} S(ud)u + \frac{1}{\sqrt{6}} A(ud)u - \frac{1}{\sqrt{3}} A(uu)d, \quad (22)$$

where  $u, d$  denote the up-, and down-quarks, and  $S(ij)$  and  $A(ij)$  are the spin-0 and spin-1 diquarks, respectively. Here we assume the  $SU(4)$  spin-flavor symmetry.

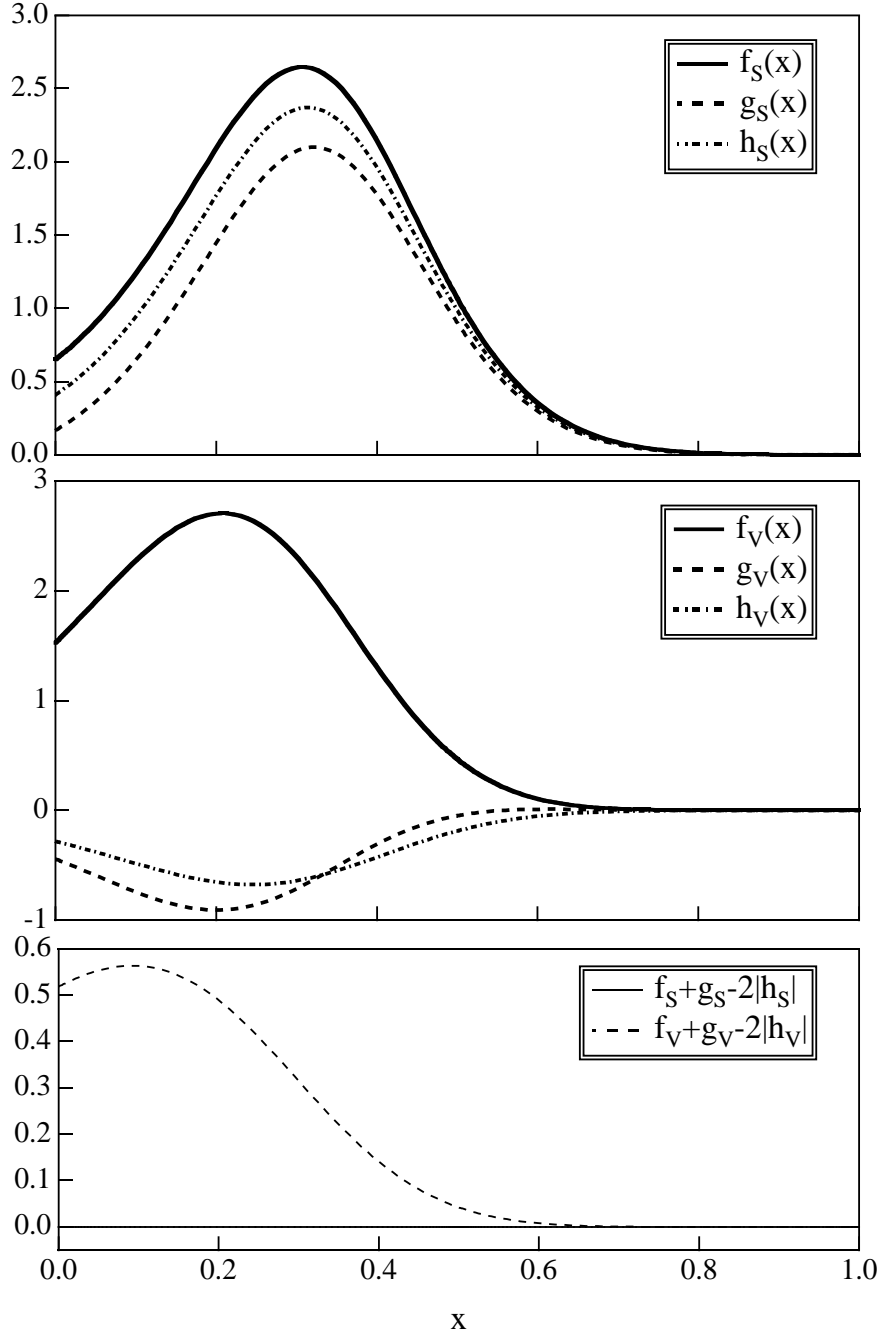


Figure 2: Quark distribution functions in the quark-diquark model of the nucleon

The upper figure shows the results of the spin-0 diquark spectator process (scalar channel), and the middle one the results of the spin-1 diquark spectator (axial-vector channel). In each figure, the quark distributions  $f_1(x)$ ,  $g_1(x)$  and  $h_1(x)$  are shown by the solid, dashed and dash-dotted curves, respectively. The lower figure shows  $f_1(x) + g_1(x) - 2|h_1(x)|$  for the scalar and axial-vector channel by the solid and dashed curves, respectively.

Quark distribution functions  $q_1^u(x)$  and  $q_1^d(x)$  with  $q = f, g, h$  are expressed as

$$q_1^u(x) = \frac{3}{2}q_S(x) + \frac{1}{2}q_V(x) , \quad (23)$$

$$q_1^d(x) = q_V(x) . \quad (24)$$

Here  $q_S$  and  $q_V$  are corresponding quark distribution functions presented in Fig.2 with the spin-0 and spin-1 diquark being spectators, respectively.

As easily seen in Eqs. (23,24), dominant contribution to the  $u$ -quark distribution comes from the spin-0 diquark spectator process, and the  $d$ -quark distribution is governed by the spin-1 diquark process. Recall that Eq. (20) implies the transversity distribution vanishes when  $m = M = 0$ ,  $h_1^u(x)$  distribution would become very small, if the chiral symmetry were not spontaneously broken.

Now we fix the model parameters with physically motivated constraints. The spin-0 diquark is expected to be tightly correlated quark-quark state due to the color spin-dependent interaction, as discussed in several works[8, 9]. In particular, experimental data of the non-leptonic hyperon weak decay require the strong correlation in the spin-0 diquark, which resolves the long standing problem of the  $\Delta I = 1/2$  rule[21, 22].

Here, we take into account differences between the spin-0 and spin-1 diquarks in the following ways. We assume that the mass difference of the diquarks is a few hundreds MeV from a consideration of the  $N$ - $\Delta$  mass splitting. Effective size of the spin-1 diquark is expected to be larger than that of the spin-0 diquark, because it is assumed to be weakly bound state of quarks. We introduce the following parametrization for the quark-diquark vertex functions[10].

$$\phi_S(k) = g_S \frac{m^2 - k^2}{(\Lambda_S^2 - k^2)^2} \quad (25)$$

$$\phi_V(k) = g_V \frac{m^2 - k^2}{(\Lambda_V^2 - k^2)^{3.5}} \quad (26)$$

Here coupling constants  $g_S, g_V$  are determined by the normalization of the unpolarized distribution  $f_1(x)$ . These functions ensure the correct behavior of the quark distributions at large  $x$ ,  $f_1^u(x) \sim (1-x)^3$  and  $f_1^d(x) \sim (1-x)^4$ , which are consistent with the standard parametrization[25]. On the other hand, such large- $x$  behavior does not agree with the parametrization of Brodsky *et al.*[26]. Recent reanalysis of the experimental data by Melnitchouk and Thomas[27], who take into account the Fermi

motion, nuclear binding and nucleon off-shell effects in the deuteron, is consistent with the QCD inspired fit by Brodsky *et al.*[26].

Taking into account above conditions, we determine the model parameters by the experimental data. We take masses of the constituents,  $m = 450\text{MeV}$ ,  $m_S = 700\text{MeV}$ , and  $m_V = 800\text{MeV}$  for the quark and diquarks. Values of the cutoff for the quark-diquark vertices are  $\Lambda_S = 0.49\text{GeV}$  and  $\Lambda_V = 0.66\text{GeV}$ .

The resulting momentum fraction carried by the  $u$  and  $d$  quarks is found to be 0.57 and 0.24 respectively, with the remaining 20% being left for the gluons and sea quarks. The spin fractions of the nucleon become  $\Delta u = 0.95$   $\Delta d = -0.30$ , which yield the nucleon axial-vector coupling  $g_A = 1.25$ . Calculated total nucleon spin is  $\Sigma = 0.65$ , which is similar with relativistic quark model calculations and larger than the empirical value. We also get the tensor charge,  $\delta u = 1.17$  and  $\delta d = -0.26$ . We have a relation  $\Delta u < \delta u$  independent of the choice of the parameters. The  $d$ -quark case is more subtle as mentioned above. We get  $|\delta d| < |\Delta d|$ , which seems to be consistent with the recent lattice result[17] and disagrees with the bag model calculation[6].

Such a tendency is quite different from the bag model result, which gives the universal inequality  $\delta q > \Delta q$  (6). In the relativistic quark potential model such as the bag model, quarks move inside the potential independently, and hence there is no correlation between the spin of the struck quark and spin structure of remaining spectator 2-quark, except for the trivial spin-isospin factor of the nucleon wave function. On the other hand, in a bound state of the quark and spin-1 diquark of the nucleon, helicities of the struck quark and spectator spin-1 diquark are correlated depending on the dynamics of the vertex function. Hence, it is rather reasonable that magnitudes of  $h_1^d(x)$  and  $g_1^d(x)$  are parameter dependent.

### 3 Momentum evolution and comparison with experiments

We have obtained the quark distribution functions in the nucleon at the low energy model scale  $\mu$ . In order to compare then with experimental data, we carry out the  $Q^2$  evolution of the distribution function with help of the perturbative QCD. It can be done by using the Altarelli-Parisi equation for  $f_1(x)$  and  $g_1(x)$ [23]. As for the transversity distribution, the Altarelli-Parisi splitting kernel is developed by Artru

and Mekhfi[18].

$$\frac{dh_1(x, Q^2)}{d(\ln Q^2)} = \frac{\alpha_s(Q^2)}{2\pi} \int_x^1 \frac{dy}{y} P_T\left(\frac{x}{y}\right) h_1(y, Q^2) \quad (27)$$

The splitting function  $P_T$  is given by,

$$P_T(z) = \frac{4}{3} \left[ \frac{2}{(1-z)_+} - 2 + \frac{3}{2} \delta(z-1) \right] \quad (28)$$

which differs from the  $f_1(x)$  and  $g_1(x)$  cases. Due to the current conservation, the 1st moments of  $f_1(x)$  and  $g_1(x)$  are unchanged by the QCD evolution. However, the 1st moment of  $h_1(x)$ , tensor charge, decreases with increasing the momentum scale.

We take the low energy model scale  $\mu^2 = 0.2\text{GeV}^2$  with the QCD cutoff  $\Lambda = 0.25\text{GeV}$ , which are adopted in Ref. [24], and use the leading order (LO) evolution equations. As discussed in section 2, the low energy effective quark model should provide quark distributions at a typical hadronic scale  $\sim 1\text{GeV}$ . However, if we adopted  $\mu = 1\text{GeV}$  as the low energy scale, the resulting distribution function would disagree with the experiment. In order to reproduce the data, the low energy scale must be smaller than  $1\text{GeV}$ , typically  $\simeq 0.5\text{GeV}$ . It is difficult to understand why such a discrepancy arises at the moment. Thus, we treat the starting scale  $\mu$  as a free parameter so as to reproduce the experiments. Inclusion of the non-trivial structure of the constituent quarks might be crucial to study the origin of this discrepancy[10], which will be discussed below.

Use of the perturbative QCD below  $1\text{GeV}$  seems to be questionable. However, inclusion of next-to-leading order (NLO) corrections modifies about  $10 \sim 20\%$  of the LO evolution result, which will be briefly discussed later. Of course, if we take much lower scale, *e.g.*  $\sim 0.1\text{GeV}^2$ , then difference of the LO and NLO results becomes very large, and the perturbative evolution is no longer reliable. All the results presented below are evolved to  $Q^2 = 10\text{GeV}^2$ . When we evolve the tensor charge from  $\mu^2 = 0.2\text{GeV}^2$  to a few  $\text{GeV}^2$  scale, the reduction of the tensor charge is less than  $20\%$ .

We first show  $f_1^u(x)$  and  $f_1^d(x)$  with the CTEQ experimental parametrization[25] in Fig.3 at  $Q^2 = 10\text{GeV}^2$  by thick-dashed and thin-dashed curves. The resulting distribution at  $x \sim 0.3$  is about  $40\%$  larger than the experimental fit. In the framework of the quark-diquark model (and most effective models), it is quite difficult to get better agreements within the reasonable parameters of the model. In the next sec-

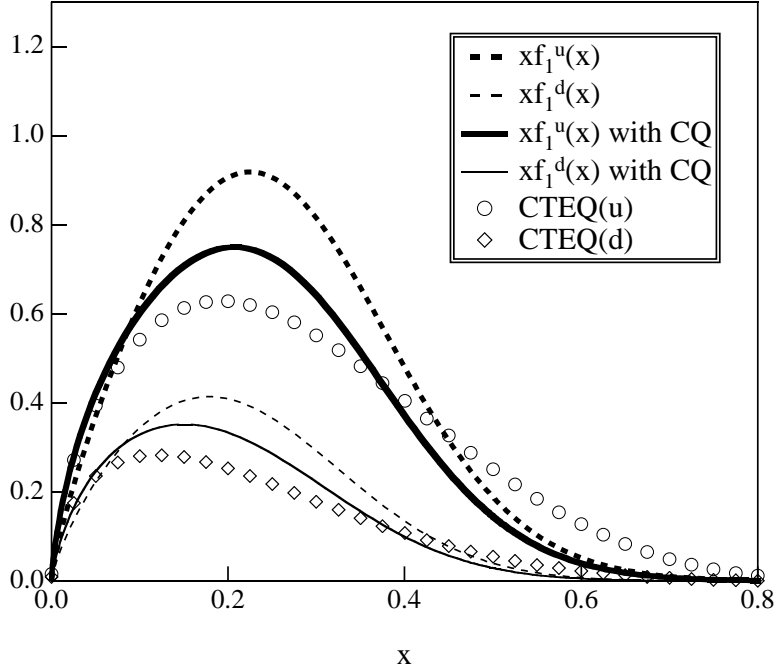


Figure 3: The unpolarized valence quark distribution of the nucleon

Unpolarized valence  $u$  and  $d$  quark distributions at  $Q^2 = 10\text{GeV}^2$ . Thick-dashed and thin-dashed curves indicate results with bare constituent quarks for  $u$  and  $d$  distributions, respectively. Results with the GS boson dressing are shown by thick-solid and thin-solid curves for  $u$  and  $d$  quarks. The circle denotes the CTEQ4 parametrization for the valence  $u$ -quark distribution, and the boxes for the  $d$ -quark[25].

tion, we will introduce dressing of the constituent quark due to the Goldstone boson cloud, which greatly improves the numerical results.

Here, we comment on the work by Kulagin *et al.* [10]. Procedure to obtain the unpolarized structure function  $f_1(x)$  presented here is the same as one of Ref. [10]. They also estimate contribution from structure of the constituent quark itself, which is described by the pion dressing at the middle- $x$  region and the Regge exchange contribution at the small- $x$ . Combining those important contributions with the bare quark-diquark model, they have obtained improved quark distributions as the input of the  $Q^2$  evolution at typical hadronic scale  $\sim 1\text{GeV}$ , at which the use of the perturbative QCD evolution is reasonably acceptable. They have reproduced observed structure function of the nucleon very well.

We have analyzed our results for the spin independent as well as the spin dependent structure function with the same parameter set used in Ref. [10]. Unfortunately,

we find resulting spin dependent structure functions become too small compared with the experimental data. This is because they adopt large diquark masses  $m_D > 1\text{GeV}$ . To reproduce the nucleon axial-vector coupling  $g_A$ , it is necessary to take smaller values of diquark masses around  $700\text{MeV}$  within this quark-diquark model, and thus impressive agreements of  $f_1(x)$  with the data are lost. Calculated distributions with our parameters also require the evolution from  $\mu^2 \sim 0.2\text{GeV}^2$  to get reasonable agreements with the data.

The longitudinal spin structure function of the proton  $G_1^p(x) = \frac{1}{2} \left[ \frac{4}{9}g_1^u(x) + \frac{1}{9}g_1^d(x) \right]$  and the neutron  $G_1^n(x) = \frac{1}{2} \left[ \frac{1}{9}g_1^u(x) + \frac{4}{9}g_1^d(x) \right]$  are shown in Fig.4. Our calculation reproduces the nucleon axial-vector coupling  $g_A = 1.25$ , but the quark spin fraction  $\Delta u = 0.95$  and  $\Delta d = -0.30$  are somewhat different from the empirical values  $\Delta u = 0.82 \pm 0.03$  and  $\Delta d = -0.43 \pm 0.03$  [28]. As a result, calculation overestimates  $g_1^p(x)$  and the total nucleon spin fraction  $\Sigma = 0.65$  compared with the empirical one  $\Sigma = 0.31 \pm 0.07$ . Note that  $g_1^d(x)$  becomes positive at the large  $x$  in this model, which is consistent with the QCD inspired parametrization of the helicity distribution functions by Brodsky *et al.*[26].

Before discussing the chiral-odd structure function, we point out the importance of ratio of the structure functions in order to extract the non-perturbative aspects of QCD from the deep inelastic data. As mentioned above, shapes of calculated quark distribution depend so strongly on the choice of the low energy scale that it is not easy to draw definite conclusions from the comparison of the model calculations with experiments. However, if we take a ratio of several distribution functions, the calculated ratio itself is rather insensitive to the choice of the scale  $\mu^2$ , since ambiguities from the evolution are considerably canceled out by taking a ratio. Therefore, we can know how non-perturbative structure of the nucleon affects the distribution functions in the deep inelastic scattering. Also, by taking a ratio, we can check internal consistency of the model calculations. Results for  $f_1^d(x)/f_1^u(x)$  and  $A_1^p = G_1^p(x)/F_1^p(x)$  presented in Fig.5 show remarkable agreements with the data. These agreements are consequence of the spin-flavor structure of the nucleon, which is incorporated by the quark-diquark model[8]. If we took un-physical values for diquark masses, *e.g.*  $m_S \geq m_V$ , agreement would be lost. Correct spin-flavor correlation of the nucleon wave function leads to a good description of these ratios.

We present  $h_1^u(x)$  and  $h_1^d(x)$  in Fig.6 at  $Q^2 = 10\text{GeV}^2$ . The  $u$ -quark distribu-

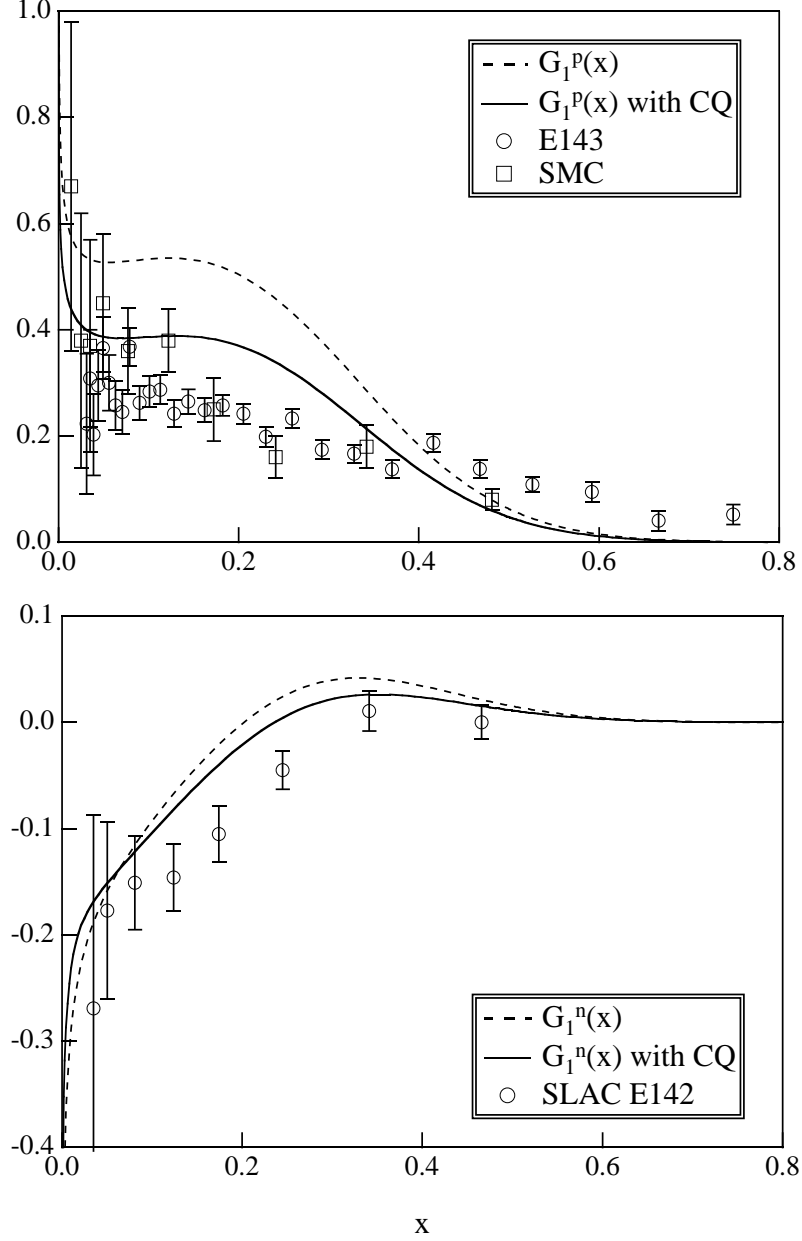


Figure 4: The longitudinal spin structure function of the proton and the neutron

Upper figure shows the proton spin structure function  $G_1^p(x)$ , and the lower one the neutron  $G_1^n(x)$  at  $Q^2 = 10\text{GeV}^2$ . In each figure, result with the bare quark is shown by the dashed curves, and one with the GS boson cloud by the solid curves. Experimental data is taken from Ref. [2].



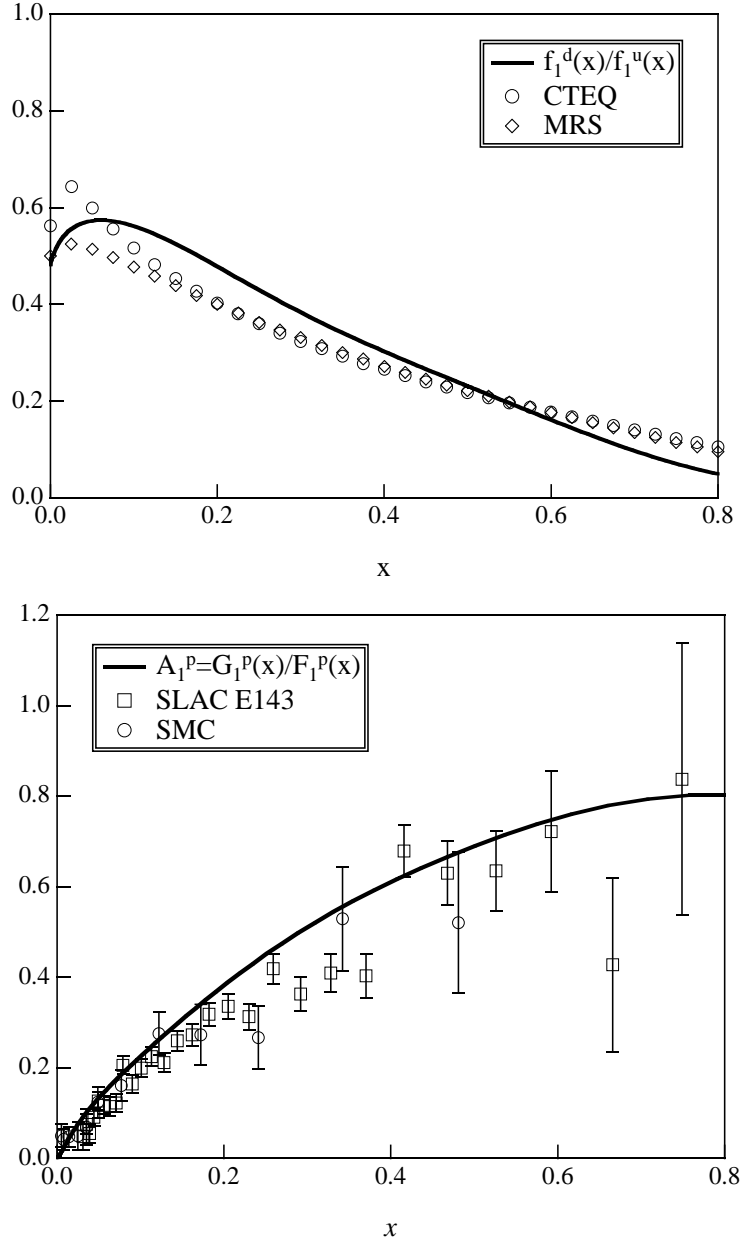


Figure 5: Ratios of the structure functions with the experimental data  $f_1^d(x)/f_1^u(x)$  and  $G_1^p(x)/F_1^p(x)$  are shown in upper and lower figures, respectively. In each figure, calculated result is shown by the solid curve with the data[25, 2].

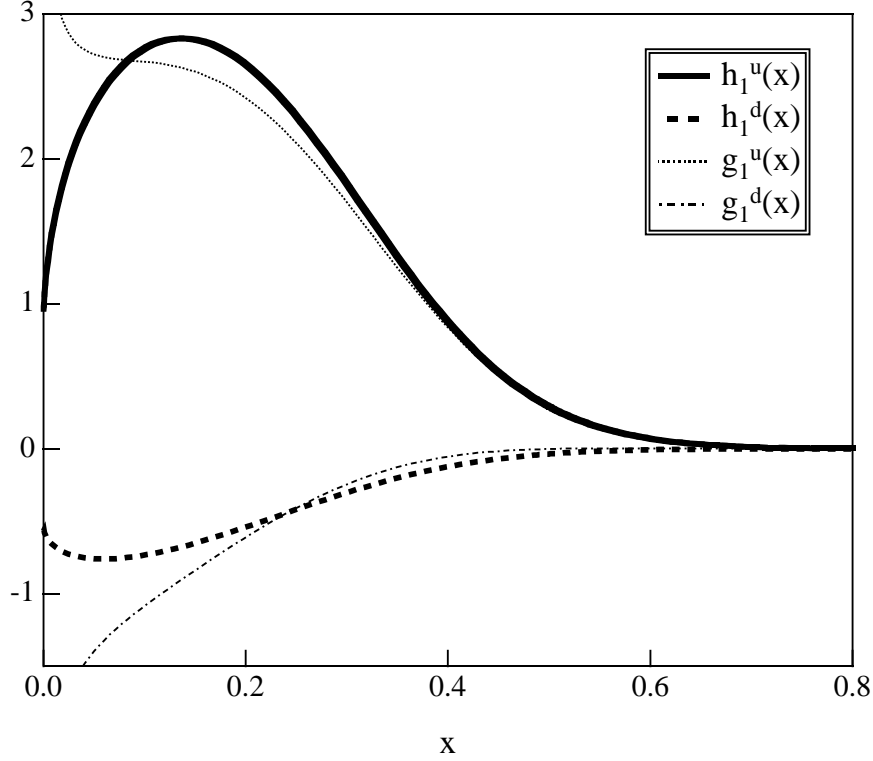


Figure 6: The transversity spin structure function  $h_1(x)$  for the  $u$  and  $d$  quarks  $h_1^u(x)$  and  $h_1^d(x)$  are displayed by the thick solid and dashed curves, respectively. For comparison,  $g_1^u(x)$  and  $g_1^d(x)$  are shown by the dotted and dash-dotted curves.

tion shows similar behavior with  $f_1(x)$  and  $g_1(x)$ , and is satisfied with  $f_1^u(x) > h_1^u(x) > g_1^u(x)$ . On the other hand, shape of the  $h_1^d(x)$  distribution differs from that of  $g_1^d(x)$ , and their magnitudes are similar. We will discuss the flavor dependence of the transversity spin distribution function in detail after introducing the GS boson dressing in the next section.

We remark that the helicity distribution functions  $g_1(x)$  becomes much larger than the transversity distributions  $h_1(x)$  at the small- $x$  region,  $x < 0.1$ . Remember that, at the low energy scale,  $g_1^u(x)$  is smaller than  $h_1^u(x)$  for all  $x$ , as shown in Fig.2. This smallness of  $h_1(x, 10\text{GeV}^2)$  at  $x < 0.1$  is due to the difference of the QCD evolution. Regarding the 1st moment of  $h_1(x)$  structure function, the splitting kernel Eq. (28) for  $h_1(x)$  does not give a significant difference, *i.e.* the reduction of the 1st moment is less than 20% by carrying out the  $Q^2$  evolution from  $\mu^2$  to  $10\text{GeV}^2$ . At small- $x$  region, however, the  $Q^2$  evolution procedure generates a quite large difference between  $g_1(x)$

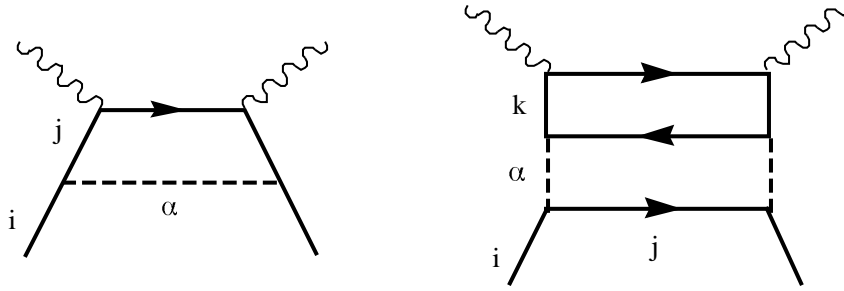


Figure 7: Goldstone boson corrections to the quark distribution function

Fig.7(a) indicates the Goldstone boson spectator process, and Fig.7(b) probes the internal structure of the Goldstone boson with the constituent quark being spectator. The constituent quark and the Goldstone boson are depicted by the solid and dashed lines, respectively.

and  $h_1(x)$ . As discussed in Ref. [29], such a difference produce great influence on the  $pp$  Drell-Yan experiment, which is planed at RHIC-SPIN. Transverse Drell-Yan spin asymmetry  $A_{TT}$  becomes substantially smaller than the longitudinal one  $A_{LL}$ , which makes it very hard to measure the transversity spin distribution function  $h_1(x)$  at RHIC.

#### 4 Corrections from the constituent quark structure

In the previous section, we treat the constituent quark as a point-like particle. Here, we shall consider contributions from the Goldstone boson dressing of the constituent quark studied in Ref. [19]. In the chiral quark model of Manohar and Georgi[30], the constituent quark interacts with the Goldstone (GS) bosons,  $\pi$ ,  $K$  and  $\eta$ , associated with the spontaneous chiral symmetry breaking. Within the one GS boson approximation, diagrams illustrated in Fig.7 contribute to the structure function. The GS boson fluctuation around the constituent quark changes probability to find a bare quark state, and gives soft contribution to the quark distribution function. Also, it changes the CQ spin structure by emitting the GS boson into the  $P$ -wave state.

The constituent quark-GS boson splitting functions giving corrections to the twist-2 structure functions are given by[19],

$$P(y)_{j\alpha/i} = \frac{g^2}{8\pi^2} \int dk_T^2 \frac{1}{y(1-y)} \frac{(m_j - m_i y)^2 + k_T^2}{y [m_i^2 - M_{j+\alpha}^2]^2} \quad (29)$$

$$\Delta P(y)_{j\alpha/i} = \frac{g^2}{8\pi^2} \int dk_T^2 \frac{1}{y(1-y)} \frac{(m_j - m_i y)^2 - k_T^2}{y [m_i^2 - M_{j+\alpha}^2]^2} \quad (30)$$

$$\delta P(y)_{j\alpha/i} = \frac{g^2}{8\pi^2} \int dk_T^2 \frac{1}{y(1-y)} \frac{(m_j - m_i y)^2}{y [m_i^2 - M_{j+\alpha}^2]^2} \quad (31)$$

for  $f_1(x)$ ,  $g_1(x)$  and  $h_1(x)$  distribution functions, respectively. Here,  $m_i, m_j, m_\alpha$  are masses of the  $i, j$ - constituent quarks and the pseudoscalar meson  $\alpha$ , respectively.  $M_{j\alpha}^2 = \frac{m_j^2 + k_T^2}{y} + \frac{m_\alpha^2 + k_T^2}{1-y}$  is the invariant mass squared of the final state. We use the quark-GS boson coupling constant  $g = 3.76$  as suggested by the effective theories[7]. These functions are calculated in the Infinite Momentum Frame,<sup>‡</sup> exponential cutoff is used with  $\Lambda_{GS} = 1.9\text{GeV}$ , which is determined to reproduce the violation of the Gottfried sum rule[19]:

$$g \rightarrow g \exp \left[ \frac{m_i^2 - M_{j\alpha}^2}{2\Lambda_{GS}^2} \right]. \quad (32)$$

In terms of these splitting functions, the quark distribution  $q_j(x)$  generated by the emission of the GS boson  $\alpha$  from a parent quark distribution  $q_i(x)$  (Fig.7(a)) is expressed as;

$$q_j(x) = \int_x^1 \frac{dy}{y} P_{j\alpha/i}(y) q_i\left(\frac{x}{y}\right) \quad (33)$$

The CQ spectator process in Fig.7(b), which contributes to the small  $x$  region, is given by,

$$q_k(x) = \int \frac{dy_1}{y_1} \frac{dy_2}{y_2} V_{k/\alpha}\left(\frac{x}{y_1}\right) P_{\alpha j/i}\left(\frac{y_1}{y_2}\right) q_i(y_2) \quad (34)$$

where  $V_{q/\alpha}(x)$  is the quark distribution function in the GS bosons. The splitting function is obtained by a symmetric relation as  $P_{\alpha j/i}(x) = P_{j\alpha/i}(1-x)$ . Since we incorporate only the pseudoscalar mesons, this diagram never contributes to the spin-dependent processes.

Combining the flavor structure of the GS bosons, one can rewrite the twist-2 structure functions renormalized by the GS boson clouds as follows,

$$f_1^u(x)_R = Z f_1^u(x) + P_{u\pi/d} \otimes f_1^d + V_{u/\pi} \otimes P_{\pi d/u} \otimes f_1^u + \frac{1}{2} P_{u\pi/u} \otimes f_1^u$$

---

<sup>‡</sup>It is possible to calculate the dressing in the covariant approach, but convolution breaking terms appear and the resulting formulae become much complicated. It is also possible to evaluate both bare distributions and dressing in the infinite momentum frame from the beginning.

$$\begin{aligned}
& + \frac{1}{4} V_{u/\pi} \otimes P_\pi \otimes (f_1^u + f_1^d) + V_{u/K} \otimes P_{K u/u} \otimes f_1^u \\
& + \frac{1}{6} P_{u\eta/u} \otimes f_1^u + \frac{1}{36} V_{u/\eta} \otimes P_\eta \otimes (f_1^u + f_1^d)
\end{aligned} \tag{35}$$

$$\begin{aligned}
f_1^{\bar{u}}(x)_R &= V_{u/\pi} \otimes P_\pi \otimes f_1^d \\
& + \frac{1}{4} V_{u/\pi} \otimes P_\pi \otimes (f_1^u + f_1^d) + \frac{1}{36} V_{u/\eta} \otimes P_\eta \otimes (f_1^u + f_1^d)
\end{aligned} \tag{36}$$

Similar expressions can be written for the  $d$ -quark case. For the spin-dependent distribution functions,

$$g_1^u(x)_R = Z g_1^u(x) + P_{u\pi/d} \otimes g_1^d + \frac{1}{2} P_{u\pi/u} \otimes g_1^u + \frac{1}{6} P_{u\eta/u} \otimes g_1^u \tag{37}$$

$$g_1^d(x)_R = Z g_1^d(x) + P_{d\pi/u} \otimes g_1^u + \frac{1}{2} P_{d\pi/d} \otimes g_1^d + \frac{1}{6} P_{d\eta/d} \otimes g_1^d \tag{38}$$

Here,  $\otimes$  expresses the convolution integral. Formulae for  $h_1(x)$  distribution are obtained by just replacing  $g$  with  $h$  in Eqs. (37),(38). The renormalization constant  $Z$  is given by,

$$Z = 1 - \frac{3}{2} \langle P_\pi \rangle - \langle P_K \rangle - \frac{1}{6} \langle P_\eta \rangle$$

where  $\langle P_\alpha \rangle$  is the 1st moment of the unpolarized splitting function. Within our model,  $Z$  is found to be 0.76. We emphasize that  $\Delta P$  is somewhat negative or nearly zero, while  $\delta P$  is positive [19]. Calculated first moments of the splitting functions for pion case are  $\langle P_\pi \rangle = 0.13$ ,  $\langle \Delta P_\pi \rangle = -0.06$  and  $\langle \delta P_\pi \rangle = 0.07$ . This sign difference of the helicity and transversity distributions causes considerable effects on the proceeding calculations.

The results for the unpolarized valence quark distribution defined by  $f_1^q(x) - f_1^{\bar{q}}(x)$  are presented in Fig.3 by using Eqs. (35, 36). Here, we show the original result by the dashed curves, and the results with the CQ structure by the solid curves. The QCD evolution procedure is the same as before with  $\mu^2 = 0.2 \text{ GeV}^2$ . The renormalization of the bare quark distribution brings down the peak of the distribution function for both  $u$  and  $d$  quarks, and the agreement around  $x \sim 0.1$  is considerably improved due to the GS boson dressing.

The GS boson contribution to  $g_1^u$  and  $g_1^d$  are different, as shown in Fig.8. As a result of the renormalization,  $g_1^u(x)$  distribution function decreases substantially, while  $g_1^d(x)$  is almost unchanged. This fact is easily understood as follows. The

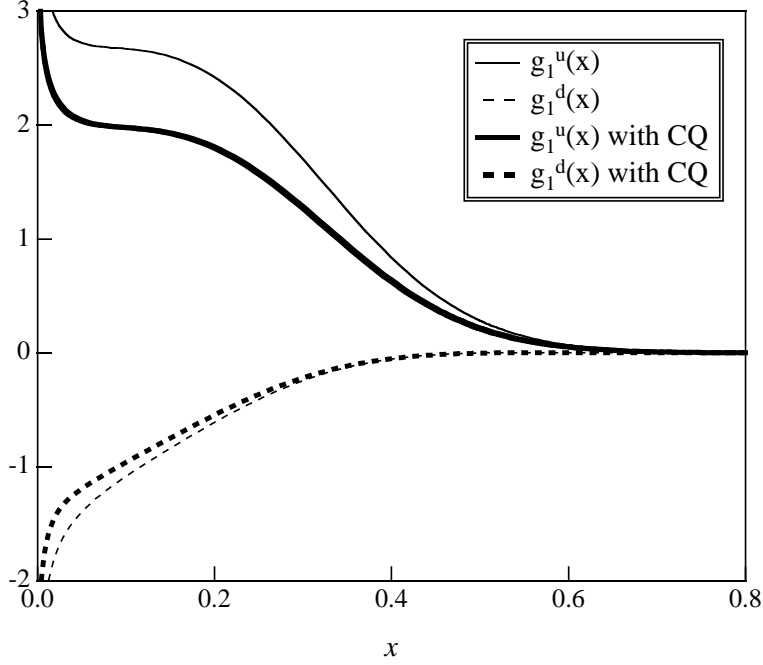


Figure 8: Helicity distribution functions  $g_1^u(x)$  and  $g_1^d(x)$  with the GS boson corrections

Results with the dressing are shown by the thick solid and dashed curves for  $u$  and  $d$  quarks, and ones without the dressing by thin curves.

renormalization factor  $Z$  always reduce absolute values of the distribution function, *i.e.* positive contribution to original (negative)  $g_1^d(x)$ . The largest correction to  $g_1^d(x)_R$ , the second term of Eq. (38)  $\Delta P_{d\pi/u} \otimes g_1^u$ , gives a negative contribution, since  $\Delta P_{d\pi/u}$  is negative. Thus, cancelation of the renormalization effect and the correction term keeps  $g_1^d(x)_R$  almost unchanged. Resulting spin fractions are tabulated in Table 1 with the original values and lattice data.

This is not the case for the transversity spin distribution. Results are shown in Fig.9 with the original ones and  $g_1^d(x)_R$  for comparison. Both  $h_1^u(x)_R$  and  $h_1^d(x)_R$  decrease, particularly, the  $d$ -quark transversity spin distribution becomes about a half of the result without the GS boson dressing. This is because the GS-boson splitting function  $\delta P$  is positive for the transversity spin case, opposite to the helicity distribution case. Hence, for the  $d$ -quark, the renormalization as well as a correction term  $\delta P_{d\pi/u} \otimes h_1^u$  are positive, which drive further reduction of the  $d$ -quark transversity spin distribution. At  $x \sim 0.1$ , the transversity spin distribution becomes the one-third of the helicity distribution. Corrected tensor charges are given in Table 1.

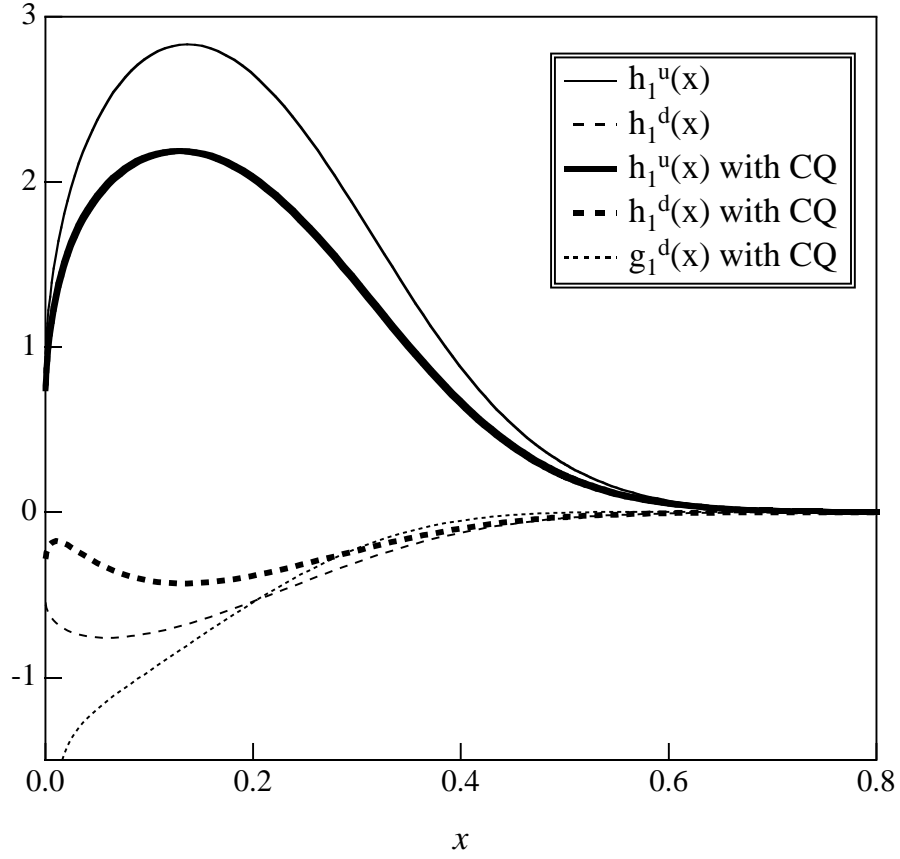


Figure 9: Transversity spin distributions  $h_1^u(x)$  and  $h_1^d(x)$  with the GS bosons  
Notations are same as those in Fig.8. We also show  $g_1^d(x)$  with the GS boson dressing by the dotted curve.

It is very interesting and important to consider experimental possibilities to measure such a flavor dependence of the transversity spin structure function. The Drell-Yan process, which is planned in RHIC-SPIN or HERA-N is not suitable to determine the flavor decomposition of the structure function, since all possible combination of  $q\bar{q}$  pair contributes to the  $\mu^+\mu^-$  cross section. On the other hand, semi-inclusive deep inelastic scattering may be a good candidate to observe the flavor dependence of the spin structure function. For example, according to the work of Kotzinian and Mulders [31], we stress the semi-inclusive deep inelastic scattering on the transversely polarized nucleon. Let us consider the  $\pi$  production process (momentum  $P_\pi$ ) on the proton target (momentum  $P$ ) with unpolarized lepton beam (momentum  $l$ ). They have found the following weighted transverse asymmetry of the cross section is related with the transversity spin distribution of the nucleon.

$$A_T(x, y, z, S_T) = \frac{\int d\phi_l \int d^2 P_{\pi\perp} \frac{|P_{\pi\perp}|}{zM_\pi} \sin(\phi_s^l + \phi_h^l) (d\sigma^+ - d\sigma^-)}{\int d\phi_l \int d^2 P_{\pi\perp} (d\sigma^+ + d\sigma^-)} \quad (39)$$

where scaling variables are given by  $x = Q^2/2P \cdot q$ ,  $y = P \cdot q/P \cdot l$ , and the momentum fraction of a produced pion  $z = P \cdot P_\pi/P \cdot q$ .  $P_{\pi\perp}$  is the transverse momentum perpendicular to  $\mathbf{q}$ , and azimuthal angles  $\phi_s^l$ ,  $\phi_h^l$  are defined with respect to the lepton plane. Asymmetry of this cross section is generated by the so called Collins effect in the fragmentation process[32]. Eq. (39) is expressed with the quark distribution and fragmentation functions as,

$$A_T(x, y, x) = -|S_T| \frac{2(1-y)}{1+(1-y)^2} \frac{h_1^a(x) H_{1\perp}^a(z)}{f_1^a(x) D_1^a(z)} \quad (40)$$

where  $h_1^a(x)$  and  $f_1^a(x)$  are the quark distribution functions, and  $D_1^a(z)$  and  $H_{1\perp}^a(z)$  unpolarized and transversely polarized quark fragmentation functions from a quark flavor  $a$  to the pion. It is well known that the  $\pi^+$  production process is dominated by the  $u$ -quark fragmentation, and  $\pi^-$  by the  $d$ -quark. Also, since pions are isospin symmetric objects, the quark fragmentation functions are the same for  $u \rightarrow \pi^+$  and  $d \rightarrow \pi^-$ . Therefore, if we take a ratio of asymmetries for  $\pi^+$  and  $\pi^-$  production processes under above assumptions, we can arrive at the following expression.

$$\frac{A_T^{\pi^-}}{A_T^{\pi^+}}(x) = \frac{h_1^d(x) f_1^u(x)}{h_1^u(x) f_1^d(x)} \quad (41)$$

where unknown ‘transversely polarized quark fragmentation function’ is canceled out.  $f_1^u(x)/f_1^d(x)$  is well determined so far, thus we can extract a ratio of the transversity



spin distribution functions of  $u$  and  $d$  quarks by counting the numbers of produced  $\pi^+$  and  $\pi^-$ . Using a similar technique with the polarized lepton beams on the longitudinally polarized proton, it may be possible to obtain a ratio of helicity distribution functions [31].

We show in Fig.10  $h_1^d(x)/h_1^u(x)$  using our calculated transversity distributions, where we can see clear flavor dependence of the spin-dependent structure functions. We also show  $g_1^d(x)/g_1^u(x)$  in our model, and one obtained by the parametrization of Brodsky *et al.*[26]. Due to the reduction of  $h_1^d(x)$ ,  $h_1^d(x)/h_1^u(x)$  is much smaller than  $g_1^d(x)/g_1^u(x)$  around  $x \sim 0.1$ . Calculated  $g_1^d(x)/g_1^u(x)$  is consistent with the parametrization of Brodsky *et al.*[26]. The bag model calculation gives similar behavior for  $h_1^d(x)/h_1^u(x)$  and  $g_1^d(x)/g_1^u(x)$ . Note that, in the naive  $SU(4)$  symmetry limit,  $h_1^d(x)/h_1^u(x) = g_1^d(x)/g_1^u(x) = -1/4$ . Alternative experimental processes to measure  $h_1(x)$  are now under investigation.

## 5 Discussions

We have studied the twist-2 quark distribution functions  $f_1(x)$ ,  $g_1(x)$  and  $h_1(x)$  of the nucleon in terms of the phenomenological quark-diquark model. We deal with the scalar and axial-vector effective nucleon-quark-diquark vertices from the symmetry consideration. Resulting distribution functions show a saturation of the Soffer's inequality  $f_1(x) + g_1(x) = 2h_1(x)$  when we use the scalar type of the quark-diquark interaction, whereas the axial-vector case is not saturated. Moreover, the spin distribution function satisfies a universal inequality  $g_1(x) < h_1(x)$  for the scalar vertex case, which is similar with result of the relativistic potential model like the bag model. On the other hand, relative size of these distribution functions depends on the model parameters in the axial-vector vertex case. With the model parameters fixed to reproduce the known observables, the quark momentum fraction and the nucleon axial-vector coupling  $g_A$ , we have found that  $|h_1(x)|$  is smaller than  $|g_1(x)|$  or they are comparable at least. Since the axial-vector case contributes to only the  $d$ -quark distribution from the  $SU(6)$  symmetry, this behavior is consistent with the recent lattice QCD calculations[17] and the QCD sum rule result[14], where the  $d$ -quark tensor charge is substantially suppressed compared with the axial-charge.

This difference simply comes from the spin structure of the quark-diquark vertices.

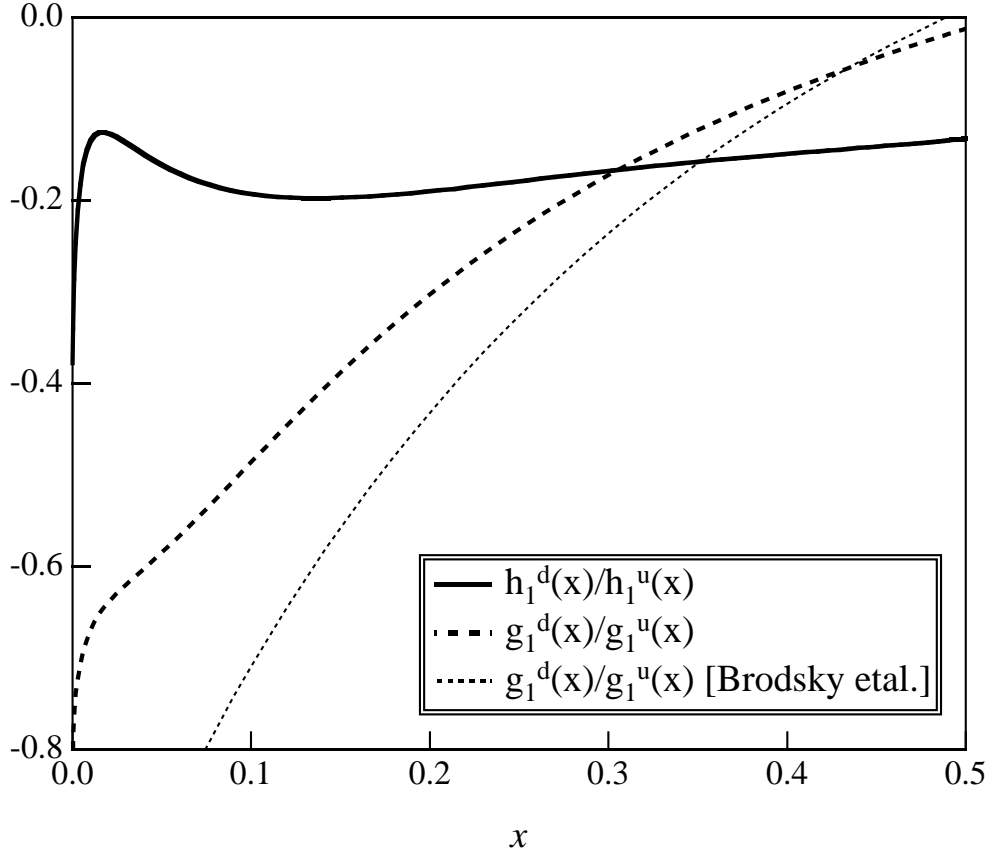


Figure 10: Flavor dependence of the spin dependent structure functions. Ratios  $h_1^d(x)/h_1^u(x)$  and  $g_1^d(x)/g_1^u(x)$  are shown by the solid and dashed curves. The QCD inspired parameterization[26] for  $g_1^d(x)/g_1^u(x)$  is also shown by the dotted curve.

We have checked other types of the Dirac structure for the vertex, and found, if the vertex is independent of the spin of the spectator diquark, *e.g.* scalar, pseudo-scalar, derivative coupling, universal relations Eqs. (5,6) hold. However, for the vector or axial-vector interactions, such relations are not realized, depending on the dynamics of the quark-diquark system.

We have also estimated corrections due to the non-trivial structure of the constituent quark itself. The constituent quark and Goldstone bosons are believed to be most important degrees of freedom below the chiral symmetry breaking scale  $\sim 1\text{GeV}$ . Corrections from the GS boson fluctuation can not be negligible, because it produces a renormalization of the CQ state as well as it changes the CQ spin structure by emitting the GS boson into the  $P$ -wave state relative to CQ. The probability to find a bare constituent quark decreases to about 70%, and the quark distribution function becomes soft. Although corrections to the spin dependent parts are parameter dependent, the GS boson fluctuation gives positive contributions to the transversity spin distribution  $h_1(x)$ , while negative for the helicity distribution  $g_1(x)$ . This feature causes further reduction of the  $d$ -quark tensor charge as shown in Table 1.

Recently, experimental methods to test the nucleon transversity spin distribution are discussed by several authors[6, 32, 33]. The transversely polarized  $pp$  Drell-Yan process is planned at RHIC, but it is suggested that the transverse double spin asymmetry becomes quite small in the accessible kinematic region at RHIC[29]. This is due to the suppression of  $h_1(x)$  at  $x < 0.1$  shown in Fig.6. This is a general result of the effective quark model calculation, if one accepts calculations of the effective theory as quark distributions at the low energy scale  $\mu \sim 0.5\text{GeV}$ . The QCD evolution procedure from  $\mu^2$  to the experimental scale generates a large difference between  $h_1(x)$  and  $g_1(x)$  at  $x < 0.1$ , even if the effective quark model provides the same inputs for  $h_1(x)$  and  $g_1(x)$ .

In Ref. [34], Artru *et al.* have given a constraint for the transversity spin distribution in the nucleon from the analysis of the single spin asymmetry in the pion production in the transversely polarized proton-proton collision  $p + p \uparrow \rightarrow \pi + X$ . Their best fit gives

$$\frac{h_1^u(x)}{f_1^u(x)} = -\frac{h_1^d(x)}{f_1^d(x)} = x^2, \quad (42)$$

which is quite different from the simple  $SU(6)$  values,

$$\frac{h_1^u(x)}{f_1^u(x)} = \frac{2}{3}, \quad \frac{h_1^d(x)}{f_1^d(x)} = -\frac{1}{3} \quad .$$

We show our numerical result in Fig.11.  $h_1^d(x)/f_1^d(x)$  and  $g_1^d(x)/f_1^d(x)$  are shown by the solid and dashed curves, and constraint from (42) by crosses. Our results are well consistent with the constraint (42) from the single pion production. The QCD parametrization of  $g_1^d(x)/f_1^d(x)$  is also shown by the circles [26]. Note that calculated distribution functions never violate the Soffer's inequality in any cases. Rather singular behavior of  $\frac{h_1^d(x)}{f_1^d(x)} = -1$  at  $x = 1$  is necessary to reproduce the observed large spin asymmetry of the  $\pi^-$  production. If we used the simple  $SU(6)$  value  $h_1^d(x)/f_1^d(x) = -1/3$ , the resulting spin asymmetry would become about a half of the experimental value[35]. It is of great interest to investigate further approach to measure the  $h_1(x)$  structure function, in particular its flavor dependence.

There are some difficulties to calculate the structure function within the effective quark model. Most serious one is use of the perturbative QCD below 1 GeV. To obtain better agreements with the experimental data, the evolution from too small scale  $\mu^2 = 0.2 \sim 0.3 \text{ GeV}^2$  is needed. We show in Fig.12  $xf_1^u(x)$  obtained by LO and NLO evolution to clarify size of higher order corrections. Here, calculations with LO and NLO evolution are displayed by the solid and dashed curves, respectively. We use the same value of  $\Lambda_{QCD}$  to calculate both LO and NLO results for simplicity, though the LO and NLO values should be in general different as found in various QCD fits of the structure function[24]. It is found that difference is about 20% of the original result, which is not significant.

Whatever difference between the NLO and LO calculations is about 20%, validity of the perturbative QCD at such a scale is still questionable. It has recently been pointed out by Kulagin *et al.*[10] that inclusion of the constituent quark structure improves this difficulty. They have shown that, if one takes into account the internal structure of the constituent quark, resulting distribution function becomes much softer. Using such improved distributions as inputs of the  $Q^2$  evolution at  $1 \text{ GeV}^2$ , where the use of perturbative QCD can be justified, they have obtained remarkable agreements with the data. Our present work is extension of their work to the spin structure function. Although we have found that their model parameters gives too small values for the spin dependent properties like  $g_A$ , such efforts contribute to right

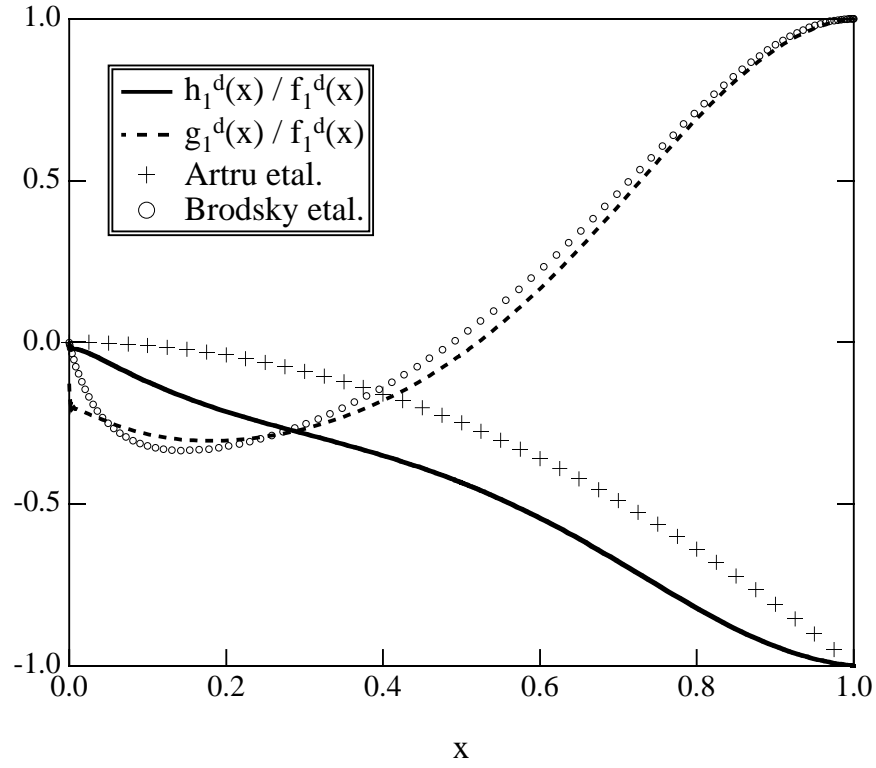


Figure 11: Ratios of spin distribution functions  $h_1^d(x)/f_1^d(x)$  and  $g_1^d(x)/f_1^d(x)$ .  $h_1^d(x)/f_1^d(x)$  and  $g_1^d(x)/f_1^d(x)$  are shown by the solid and dashed curves, respectively. Best fit parameterization for  $h_1^d(x)/f_1^d(x)$  extracted from the single spin asymmetry of the pion production in the polarized  $pp$  collision[34] is also shown by the crosses. The circles denote the parameterization of Brodsky *et al.* for  $g_1^d(x)/f_1^d(x)$  [26].

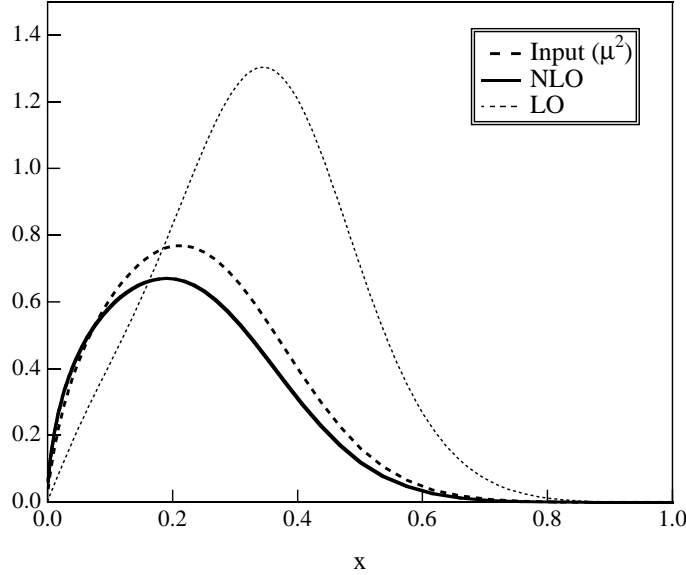


Figure 12: Comparison of LO and NLO QCD evolution

Results for unpolarized  $u$ -quark distribution functions with the NLO and LO  $Q^2$  evolution are shown by the solid and dashed curves.

direction to overcome this difficulty.

Our aim is to investigate the non-perturbative nucleon structure from studies of the quark distributions measured in the high energy experiments. Obtained suppression of the  $d$ -quark tensor charge is a key to understand how the real nucleon structure differs from the simple bag model-like structure. Future experimental efforts will clarify spin-flavor structure of the nucleon.

## Acknowledgments

K.S. would like to thank W. Weise for reading of a manuscript and a collaboration of Ref. [19], where corrections to the quark distributions from the Goldstone boson dressing are studied. This work is supported in part by the Alexander von Humboldt foundation.

## References

- [1] J.J. Aubert *et al.*, European Muon Coll., Nucl. Phys. **B293** (1987) 740
- [2] P. Anthony *et al.* SLAC E-142, Phys. Rev. **D54** (1996) 6620  
D. Adams *et al.* (SMC), Phys. Lett. **B329** (1994) 399  
K. Abe *et al.* (SLAC E143), Phys. Rev. Lett. **74** (1995) 346, Phys. Rev. Lett. **75** (1995) 25
- [3] D.A. Adams *et al.*(SMC), Phys. Lett. **B336** (1994) 125  
K. Abe *et al.*(E143), Phys. Rev. Lett. **76** (1996) 587
- [4] M. Anselmino, A. Efremov, E. Leader, Phys. Rep. **261** (1995) 1
- [5] J.P. Ralston and D.E. Soper, Nucl. Phys. **B152** (1979) 109
- [6] R.L. Jaffe and X. Ji, Nucl. Phys. **B375** (1992) 527
- [7] Y. Nambu and G. Jona-Lasinio, Phys. Rev. **122** (1961) 345  
For reviews, T. Hatsuda and T. Kunihiro, Phys. Rep. **247** (1994) 221  
U. Vogl and W. Weise, Prog. Part. Nucl. Phys. **27** (1991) 195
- [8] H. Meyer and P.J. Mulders, Nucl. Phys. **A528** (1991) 589  
W. Melnitchouk, A.W. Schreiber, A.W. Thomas, Phys. Rev. **D49** (1994) 1183
- [9] K. Suzuki, T. Shigetani, H. Toki, Nucl. Phys. **A573** (1994) 541
- [10] W. Melnitchouk and W. Weise, Phys. Lett. **B334** (1994) 275  
S.A. Kulagin *et al.*, Nucl. Phys. **A597** (1996) 515, and references therein
- [11] K. Kusaka, G. Piller, A.W. Thomas, A.G. Williams, hep-ph/9609277
- [12] B.L. Ioffe and A.Yu. Khodjamirian, Phys. Rev. **D51** (1995) 3373
- [13] V. Barone, T. Calarco and A. Drago, hep-ph/9605434
- [14] H. He and X. Ji, Phys. Rev. **D52** (1995) 2960, *ibid* **D54** (1996) 6897
- [15] J. Soffer, Phys. Rev. Lett. **74** (1995) 1992
- [16] G.R. Goldstein, R.L. Jaffe, X. Ji, Phys. Rev. **D51** (1995) 3373

- [17] S. Aoki, M. Doui, T. Hatsuda, Y. Kuramashi, UTHEP-339, hep-lat/9608115  
M. Göckeler *et al.*, DESY 96-152, hep-lat/9609039
- [18] X. Artru and M. Mekhfi, Z. Phys. **C45** (1990) 669 (1977) 298
- [19] K. Suzuki and W. Weise, TU-Munich preprint
- [20] R.L. Jaffe and G.G. Ross, Phys. Lett. **B93** (1980) 313
- [21] H.G. Dosch, M. Jamin and B. Stech, Z. Phys. **C42** (1989) 167
- [22] K. Suzuki and H. Toki, Mod. Phys. Lett. **A9** (1994) 1059
- [23] G. Altarelli and G. Parisi, Nucl. Phys. **B126** (1977) 298
- [24] M. Glück, E. Reya and A. Vogt, Z. Phys. **C48** (1990) 471
- [25] H.L. Lai *et al.*, Phys. Rev. **D51** (1995) 4763
- [26] S.J. Brodsky, M. Burkhardt, I. Schmidt, Nucl. Phys. **B441** (1995) 197
- [27] W. Melnitchouk and A.W. Thomas, Phys. Lett. **377** (1996) 11
- [28] J. Ellis and M. Karliner, Phys. Lett. **B341** (1995) 39
- [29] V. Barone, T. Calarco and A. Drago, hep-ph/9702239
- [30] A. Manohar and H. Georgi, Nucl. Phys. **B234** (1984) 189
- [31] A.M. Kotzinian and P.J. Mulders, hep-ph/9701330  
P.J. Mulders and R.D. Tangerman, Nucl. Phys. **B461** (1996) 197
- [32] J.C. Collins, Nucl. Phys. **B396** (1993) 161
- [33] X. Ji, Phys. Rev. **D49** (1994) 114  
X. Artru, hep-ph/9512238
- [34] X. Artru, J. Czyzewski, H. Yabuki, Z. Phys. **C73** (1997) 527
- [35] D.L. Adams *et al.*, Phys. Lett. **B264** (1991) 463



## Table Captions

Table 1

The first moments of the helicity and transversity distribution functions (at  $\mu^2$ ). The axial charges  $\Delta u$  and  $\Delta d$  are shown in the second and third columns, and corresponding tensor charges are given in the forth and fifth columns, respectively. Results of with the bare CQ and dressed CQ are displayed in the second and third rows. Experimental data, lattice calculations and QCD sum rule results are shown in the third, forth and fifth rows, respectively.

**Table 1**

	$\Delta u$	$\Delta d$	$\delta u$	$\delta d$
Bare	0.95	-0.30	1.17	-0.26
With CQ	0.73	-0.25	0.92	-0.15
Exp[28]	$0.83 \pm 0.03$	$-0.43 \pm 0.03$	—	—
Lattice[17]	0.76	-0.35	0.84	-0.23
Sum rule[14]			$1.33 \pm 0.53$	$-0.04 \pm 0.02$